Development of a WCMS-HSPF Groundwater Model Component for Underground Mine Hydrologic Impact Assessment

OSM-NTTT Applied Science Cooperative Agreement S07AZ12498

Fiscal Year 2007

Final Project Report

Natural Resource Analysis Center
West Virginia University

October 31, 2009

Introduction

The Natural Resources Analysis Center (NRAC) Watershed Characterization and Modeling System (WCMS) is an analysis tool widely used within the West Virginia Department of Environmental Protection (WVDEP) for a variety of applications related to water resource management (Fletcher, et al., 2004). Recently, WCMS capabilities were expanded with development of a new toolbar to support the application of the U.S. Environmental Protection Agency HSPF (Hydrologic Simulation Program-Fortran, Bicknell, et al., 2001) watershed hydrology and surface water quality model, which is a component of the EPA BASINS watershed management system (USEPA, 2001). WCMS provides specific GIS interface functionality that substantially automates the application of HSPF to mine-impacted watersheds, significantly reducing the complexity of watershed modeling analyses needed to evaluate new coal mine permit applications (Eli, et al., 2004, 2005). Additionally, a new model component has been developed to include the impacts of the proposed surface mine site hydrology, including the drainage plan design and NPDES (National Pollutant Discharge Elimination System) outflow points (Lamont, et al., 2005). Currently, WCMS-HSPF has been calibrated for use on 235 trend station watersheds within West Virginia by jointly calibrating five representative watersheds that share similar surface land use/vegetative cover, soils, topography, and geology with the trend station watersheds. Trend station watersheds have been defined by the WVDEP at stream locations where regular water quality monitoring is conducted.

WCMS-HSPF models the surface rainfall-runoff components of the hydrologic cycle. The subsurface is not explicitly modeled in HSPF, and therefore, the geologic structure and hydraulic characteristics of the subsurface, including the impacts of underground mines on the local and regional groundwater system, are not included. Conversely, the USGS MODFLOW groundwater model (Harbaugh, 2005) has been used to model the impacts of underground mining on groundwater systems (Sahu, 2003; Capo, 2004). MODFLOW is universally accepted as a standard for groundwater modeling as is HSPF for surface water modeling. The idea of combining the two to form a complete water basin modeling system is not new.

MODFLOW provides a three dimensional finite difference solution of the governing differential equations of saturated groundwater flow. It can simulate unsteady flow in irregular shaped flow systems in which aquifer layers can be confined, unconfined, or a combination of

the two. Flow to wells, spatially distributed recharge, evapotranspiration, flow to drains, and flow exchange with rivers can all be included in the simulation. Hydraulic conductivities for any layer may differ spatially and be anisotropic (dependent on direction). Boundary conditions must be specified for the outer boundary grid cells in the form of a known hydraulic gradient, or by use of specified external inflows or outflows. MODFLOW requires extensive data preparation and entry and is commonly used in conjunction with pre- and post-processing graphic interface software, such as GMS (Groundwater Modeling System) or Visual MODFLOW (for examples see http://www.scisoftware.com.)

Since HSPF is primarily a surface water hydrologic model and MODFLOW is primarily a groundwater model, it is apparent that using the two in combination permits a more holistic approach to modeling drainage basins. In 1988, the Florida Institute of Phosphate Research (FIPR) funded a project to develop a combined hydrologic modeling system to provide a predictive capability of the interactions of surface water and ground water for the lowlands of Florida, where shallow water table aquifers are located near the surface. The FIPR Hydrologic Model (FHM), containing both HSPF and MODFLOW as primary components, was developed by a team of researchers that included the University of South Florida (Ross, et al., 1997). FHM has since evolved into a public domain version named Integrated Hydrologic Model (IHM) (Ross, et al., 2004). A number of studies using IHM have resulted in publications (Trout, et al., 2003; Hosseinipour, 2003, Aly, 2005; Ross, et al., 2005).

As shown in Figure 1, IHM (and its predecessor FHM) was developed for applications in Florida where the land is flat and the water table is near the surface. The HSPF-MODFLOW interface in IHM uses GIS-based tools to translate between the stream segment and sub-watershed polygon-based spatial data structure of HSPF and the grid cell structure of MODFLOW. Additionally, the computational time scales of HSPF and MODFLOW are incompatible since HSPF computes at hourly increments or less, while MODFLOW uses time increments of days, or longer. IHM provides the integration required to allow each model to operate using its own spatial-temporal structure while still being able to exchange data effectively. A limitation of IHM (which will not be shared by the proposed RGRM/MODFLOW component) requires that MODFLOW must underlay the full spatial extent of the HSPF surface model.

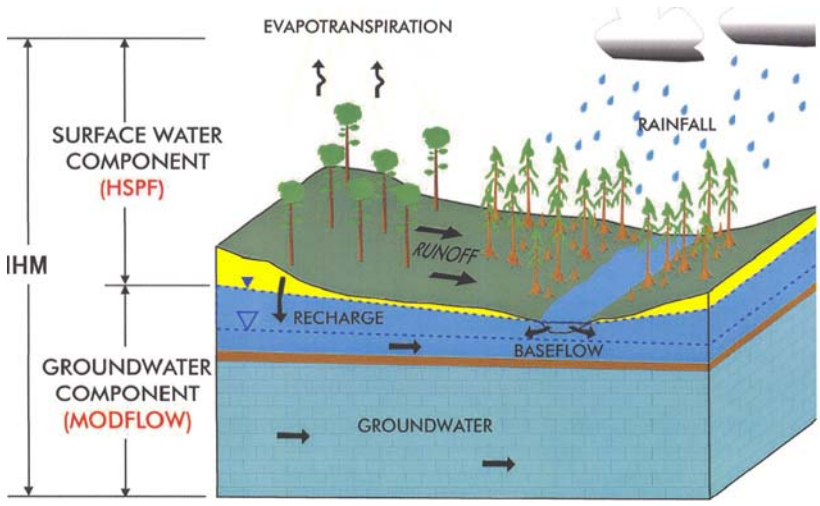

Figure 1. Combined Surface and Groundwater Modeling Provided by IHM (Integrated Hydrologic Model; Ross, et al., 2004)

The Integrated Hydrologic Model (IHM) is impractical for use in conjunction with WCMS in West Virginia due to differences in ground water regimes and data structures. Development of a Regional Groundwater Recharge Model (RGRM) that is compatible with WCMS-HSPF and the underlying SLW (segment-level watershed) data structure of WCMS has been initiated to provide a more parsimonious solution to the groundwater modeling need in the coal mining areas of West Virginia. The development plan for the RGRM component supports the optional use MODFLOW as the primary underground mine site hydrologic model, imbedded within the much larger regional groundwater system modeled by RGRM. Since the RGRM component is to be run jointly with HSPF, and is also to be pre-calibrated to all trend station watersheds, it may be more accurately described as an extended HSPF capability rather than a separate groundwater modeling system. It will provide a broad-brush, approximate picture of the trend station watershed groundwater system opposed to that potentially provided by the more detailed modeling capabilities of MODFLOW.

The IHM (discussed above) can provide significant guidance in the details of joint use of HSPF and MODFLOW, but it cannot be directly applied in the terrain represented in Figure 2. IHM was designed for lowland topography where water tables are near the surface. More importantly, IHM requires that the spatial extent of HSPF and MODFLOW match over the entire water basin being modeled. This latter requirement would be much more difficult to implement

in Appalachian coal fields were the groundwater systems are much more complex and spatially varied, and the rugged topography results in outcrops and perched water tables. MODFLOW has been successfully applied to individual underground mine groundwater impact analyses in the Appalachian region (see earlier references), but usually only in the saturated zone corresponding to that below the local water table (below drainage).

The development plan for the WCMS-HSPF Regional Groundwater Recharge Model (RGRM) component supports the use MODFLOW as the optional underground mine site hydrologic model, imbedded within the much larger regional groundwater system simulated by RGRM. Any current operating environment for MODFLOW could potentially be used, such as GMS or Visual MODFLOW. Since the RGRM component is to be run jointly with HSPF and is also to be pre-calibrated to all trend station watersheds, it can be considered as an extended HSPF capability, rather than as a separate groundwater modeling system. It will provide a broad-brush, approximate picture of the trend station watershed groundwater system as opposed to that provided by the more detailed modeling capabilities of MODFLOW.

This report concludes the first phase development of RGRM as part of a three phase design, development, and implementation project that will extend the current surface water modeling capability of WCMS into the groundwater domain. The design and testing of the basic model structure has been completed. Year 2 (continuation funding has been denied) was to have added WCMS toolbars to implement the RGRM model functionality and its ability to represent underground mine cavities, mine pools, and vertical fracture impacts on aquifer dewatering and streamflow. Year 3 (also not to be funded) would have completed verification testing, user training, and installation of the latest version of WCMS-HSPF-RGRM on the user network at WVDEP.

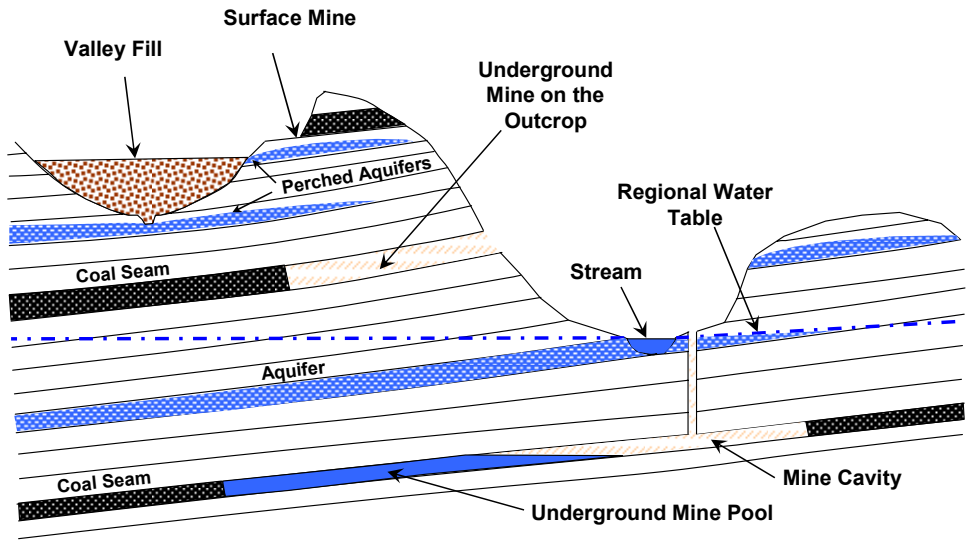

Figure 2. Schematic Geologic Cross Section Showing Relative Positions of Mined Coal Seams and Groundwater Features.

Methodology

RGRM Spatial Data Structure

The WCMS GIS database will be expanded to include new spatial attribute data required for support of RGRM. WCMS maintains a statewide database of 1:24,000 scale NHD (National Hydrography Dataset) stream segments (reaches), and the associated DEM (30 m resolution, re-sampled to 20 m). Other existing data layers include land use/cover, surface drainage information, and the SLW (Segment Level Watershed) polygons associated with each NHD stream segment. A typical stream network example with the associated SLW's is illustrated in Figure 3 for the East Fork Twelve Pole Creek watershed (southwestern WV). The SLW's are the highest resolution HRUs (Hydrologic Response Units) consistent with the NHD network, and are to be used as the primary level of spatial subdivision within the RGRM component.

Delaunay triangulation of the NHD SLW area centroids, as shown in Figure 4, establishes a network of connected points (nodes) from which Voronoi polygons (MATLAB, Mathworks, 2005) are constructed (Figure 5). The Delaunay triangulation establishes the spatial connectivity of the aquifer layers across the entire water basin being simulated via the triangulated irregular network (TIN) interconnections between nodes. The lateral boundary of

the control volume for maintaining the conservation of mass in each SLW aquifer layer corresponds to the actual boundary of that SLW and not the Voronoi polygon boundary. The Voronoi polygon sides are used to compute the directional flow cross section areas while the Delaunay triangle sides (links) are used to establish flow direction connectivity and to compute hydraulic gradients between adjacent SLWs. The connecting network of links is assumed to convey groundwater much the same way as pipes conveying water in a pipe flow network. The pipe network analogy allows a 2-dimensional model to be constructed using a one dimensional energy equation formulation (Darcy's law) within a set of algebraic equations that assure conservation of mass (groundwater) within each polygon. This approach, originally proposed by Narasimhan and Witherspoon (1976), significantly simplifies the solution for the piezometric head within each SLW. It should be noted that the flow in the imaginary pipe network does not reflect the actual groundwater flow vector map. The groundwater flow vectors can be generated in a post-processing step using the smoothed 3-dimensional piezometric surface for each aquifer layer.

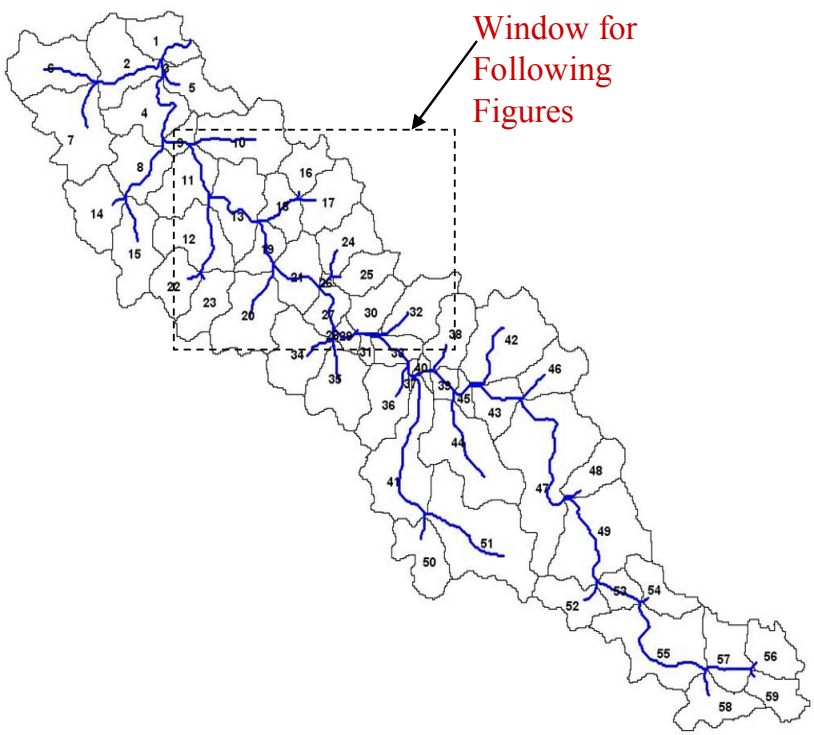

Figure 3. East Fork Twelve Pole Creek Stream Network and Associated Segment-Level Watersheds (SLW).

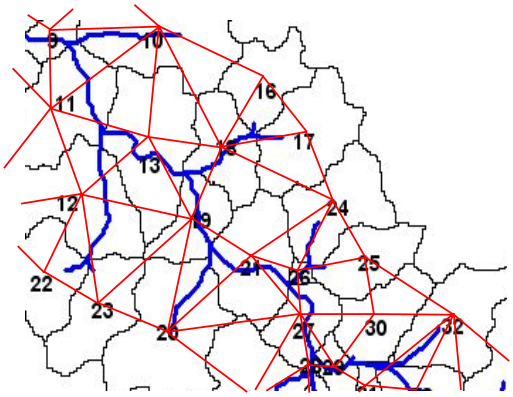

Figure 4. Delaunay Triangulation using the SLW Centroids.

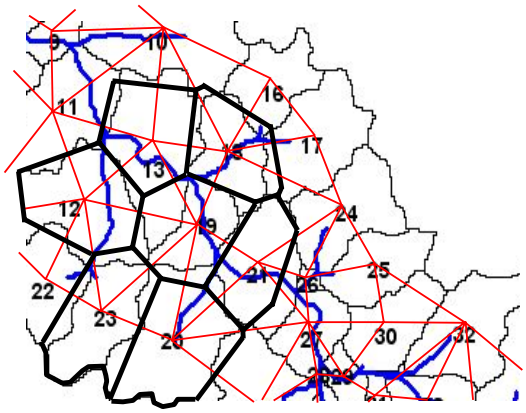

Figure 5. Voronoi Polygons Constructed Surrounding Segment-Level Watershed 19.

As shown in Figures 4 and 5, the groundwater domain is subdivided into Voronoi polygons in the horizontal plane at a scale consistent with the Segment Level Watersheds (SLW) contained in the WCMS database. At the 1:24,000 scale of the NHD (National Hydrography Dataset), SLW areas average approximately 60 ha (150 acres). As shown in Figure 6, additional horizontal resolution to represent underground mine cavities or other small features such as fault lines and fractures can be achieved by adding additional local control points to adjust size and location of the Voronoi polygons they create, and the flow directions between the polygon centroids.

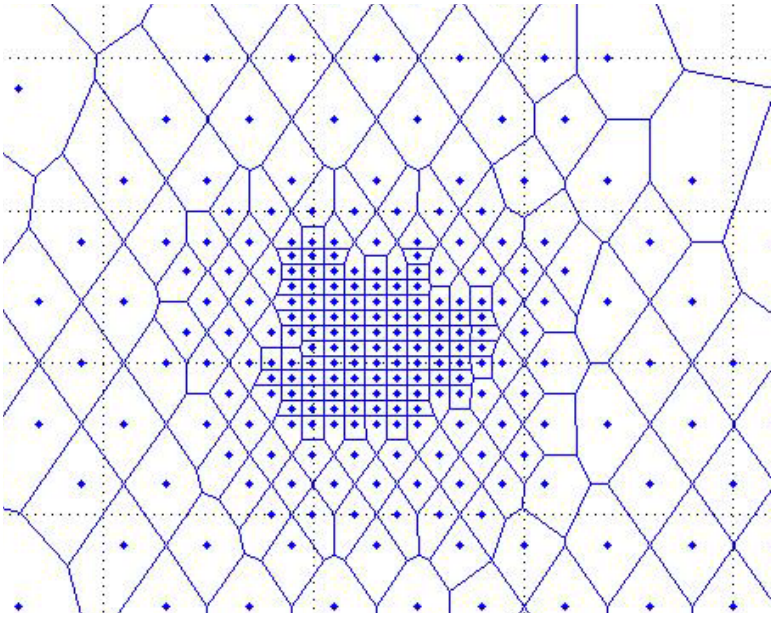

Figure 6. Additional control points define local subsurface features such as mines.

Single Layer Model Formulation

Initially, a single layer model was developed and tested with the flow assumed to be predominantly horizontal. Therefore a single equivalent horizontal hydraulic conductivity value was used for each flow direction and the aquifer was assumed to be unconfined with horizontal flow behavior according to the Dupuit assumption (Bear and Verruijt, 1987). The continuity equation is written for each connecting node (SLW centroid) in the Delaunay triangulation (Equation 1). Figure 7 illustrates the application of Equation 1 to a representative SLW.

$$\sum_j Q_{ij} - Q_i^* + I_i A_i^* = \frac{dS_i}{dt} = \frac{d\left(h_i A_i^* \eta_i\right)}{dt} = A_i^* \eta_i \frac{dh_i}{dt}$$

where:

$Q_{ij} =$ inflow to node i from adjacent node j $\left[m^3/d\right]$

$Q_i^* =$ outflow to SLW i stream segment $\left[m^3/d\right]$

$I_i =$ recharge rate in SLW i $\left[m/d\right]$ (1)

$A_i^* =$ SLW i planform area $\left[m^2\right]$

$S_i = h_i A_i^* \eta_i =$ SLW i groundwater storage volume $\left[m^3\right]$

$h_i =$ aquifer saturated thickness in SLW i $\left[m\right]$

$\eta_i =$ drainable porosity in SLW i

$t =$ time $\left[d\right]$

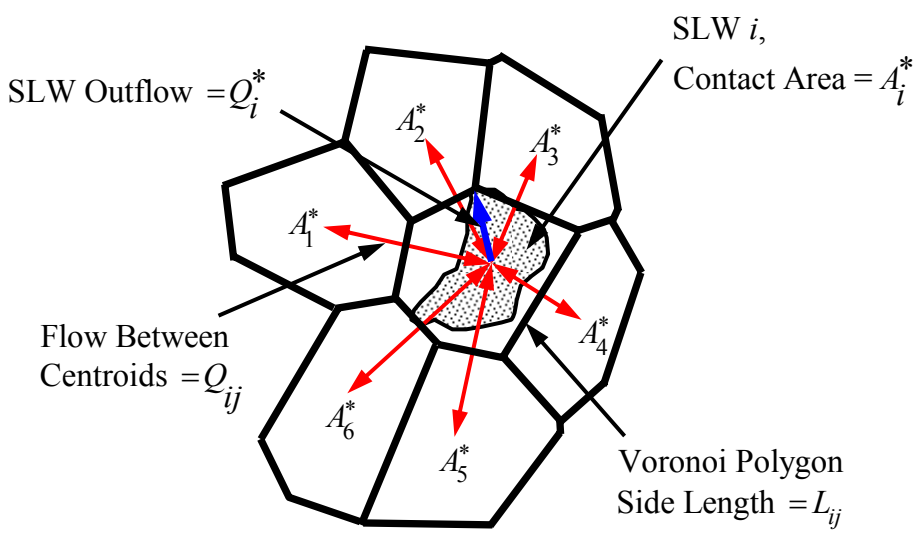

Figure 7. Groundwater flow exchange between the focus SLW and surrounding SLW's.

It should be noted that the summation sign convention in Equation 1 assumes that inflows to node i are positive and outflows are negative. Additionally, it is assumed that the drainable porosity η_i is equal to the specific yield as it is customarily defined in water table aquifers. The

energy equation is written along each link (triangle side) of the Delaunay triangulation (Equation 2).

$$Q_{ij} = K_{ij} A_{ij} \frac{d\phi_{ij}}{dl_{ij}}$$

where:

$Q_{ij} =$ flow from node j to node i $\left[m^3/d \right]$

$K_{ij} =$ hydraulic conductivity along link ij $\left[m/d \right]$ (2)

$A_{ij} =$ flow cross section area along link ij $\left[m^2 \right]$

$\phi_{ij} =$ piezometric level along link ij $\left[m \right]$

$\frac{d\phi_{ij}}{dl_{ij}} =$ piezometric gradient from node i to node j along link ij

$l_{ij} =$ link ij length $\left[m \right]$

The sign convention for the direction of flow Q_{ij} remains the same as in Equation 1. The flow cross section area A_{ij} is computed as a product of the Voronoi polygon side length L_{ij} bisecting link ij and the mean aquifer saturated thickness $\left(h_i + h_j \right)/2$ at that point. A special form of the energy equation is used to compute the outflow from SLW i to its stream segment Q_i^* (Equation 3).

$$Q_i^* = K_i^* A_i^* \frac{d\phi_i}{dl_i^*} \approx 2K_i^* \sqrt{A_i^*} \left(\phi_i - z_i^* \right)$$

where:

$\frac{d\phi_i}{dl_i^*}$ is approximated by $\frac{\left(\phi_i - z_i^* \right)}{\sqrt{A_i^*}/2}$

and where

$z_i^* =$ elevation of the outflow end of stream segment i $\left[m \right]$ (3)

$\phi_i =$ piezometric level in SLW i $\left[m \right]$

$l_i^* =$ flow length from centroid of SLW i to its outlet point $\left[m \right]$

$K_i^* =$ effective outflow hydraulic conductivity within SLW i $\left[m/d \right]$

$\sqrt{A_i^*}/2 =$ effective flow length from SLW i to its outlet point $\left[m \right]$

the remaining variables are defined as above

A backward in time finite difference equation can now be written for Equation 1 for each node *i* in the network (Equation 4).

$$\frac{\left(\sum_j Q_{ij} - Q_i^* + I_i A_i^*\right)^{t-\Delta t} + \left(\sum_j Q_{ij} - Q_i^* + I_i A_i^*\right)^{t}}{2} = A_i^* \eta_i \frac{\left(h_i\right)^t - \left(h_i\right)^{t-\Delta t}}{\Delta t} \tag{4}$$

Equation 2 can also be expressed in finite difference form along each link *ij* in the network (Equation 5).

$$\left(Q_{ij}\right)^t = K_{ij}\left(A_{ij}\right)^t \frac{\left(\phi_j - \phi_i\right)^t}{l_{ij}}$$

or

$$\left(Q_{ij}\right)^{t-\Delta t} = K_{ij}\left(A_{ij}\right)^{t-\Delta t} \frac{\left(\phi_j - \phi_i\right)^{t-\Delta t}}{l_{ij}} \tag{5}$$

where:

$A_{ij} = \frac{h_i + h_j}{2} L_{ij}$

$L_{ij} =$ Voronoi polygon side length bisecting link *ij* $[m]$

In Equation 5 it is important to note that if A_{ij} is evaluated at the same time step as the piezometric head ϕ, a nonlinear equation in the unknown piezometric head ϕ results at time step *t*. In the numerical procedure the nonlinear equation is avoided by using the flow area A_{ij} from the preceding time step. Substituting Equation 5 into Equation 4, and assuming that zero elevation datum corresponds to the aquifer bottom (then $h = \phi$), Equation 6 results.

$$\left[-\sum_j\left(\frac{K_{ij}\left(A_{ij}\right)^t}{2l_{ij}}\right)-K_i^*\sqrt{A_i^*}-\frac{A_i^*\eta_i}{\Delta t}\right]\left(\phi_i\right)^t+\sum_j\left(\frac{K_{ij}\left(A_{ij}\right)^t\left(\phi_j\right)^t}{2l_{ij}}\right)=$$
$$\left[\sum_j\left(\frac{K_{ij}\left(A_{ij}\right)^{t-\Delta t}}{2l_{ij}}\right)+K_i^*\sqrt{A_i^*}-\frac{A_i^*\eta_i}{\Delta t}\right]\left(\phi_i\right)^{t-\Delta t}-\sum_j\left(\frac{K_{ij}\left(A_{ij}\right)^{t-\Delta t}\left(\phi_j\right)^{t-\Delta t}}{2l_{ij}}\right) \tag{6}$$
$$-2K_i^*\sqrt{A_i^*}\phi_i^*-\left(\frac{\left(I_i\right)^{t-\Delta t}+\left(I_i\right)^t}{2}\right)A_i^*$$

The piezometric heads ϕ at time step *t* on the left hand side of Equation 6 are to be calculated as a function of the known quantities on the right side. Equation 6 is written for each SLW centroid (Delaunay triangle vertex) in the polygon network, yielding N equations in N unknown piezometric heads. Solution of the system of N equations is accomplished using matrix methods at each time step in the simulation. Following determination of the piezometric heads, connecting link flows and node outflows (to the stream segments) can be computed using Equations 3 and 5 for each time step.

Single Layer Model - Steady State Formulation

A steady state solution for the piezometric heads is often desired for a particular set of steady state boundary conditions (code verification in this case). This can be accomplished by simply running the unsteady simulation (using Equation 6) for a sufficient period of time steps for the solution to approach a steady state. However, this approach is inefficient since a large number of time steps will typically be required. The continuity equation (Equation 1) can be rewritten for the steady state solution, resulting in Equation 7.

$$\sum_j Q_{ij}-Q_i^*+I_iA_i^*=0 \tag{7}$$

Equations 2 and 3 remain unchanged. Substituting Equations 2 and 3 into Equation 7 results in Equation 8.

$$\sum_j \left(K_{ij} A_{ij} \frac{d\phi_{ij}}{dl_{ij}} \right) - K_i^* A_i^* \frac{d\phi_i}{dl_i^*} + I_i A_i^* = 0 \tag{8}$$

A finite difference form of Equation 8 can be written using the iteration index *n* (Equation 9).

$$\sum \left(K_{ij} \left(A_{ij} \right)_{n-1} \frac{\left(\phi_j - \phi_i \right)_n}{l_{ij}} \right) - K_i^* A_i^* \frac{\left(\phi_i - z_i^* \right)_n}{\sqrt{A_i^*}/2} + I_i A_i^* = 0$$

where (9)

$$A_{ij} = \frac{h_i + h_j}{2} L_{ij}$$

Equation 9 can be expanded to a form more convenient for writing N linear equations in N unknown piezometric heads at iteration *n* (Equation 10).

$$\left[-\sum_j \left(\frac{K_{ij} \left(A_{ij} \right)_{n-1}}{l_{ij}} \right) - 2K_i^* \sqrt{A_i^*} \right] \left(\phi_i \right)_n + \sum_j \left(\frac{K_{ij} \left(A_{ij} \right)_{n-1} \left(\phi_j \right)_n}{l_{ij}} \right) = -2K_i^* \sqrt{A_i^*} z_i^* - I_i A_i^*$$

where (10)

$$A_{ij} = \frac{h_i + h_j}{2} L_{ij}$$

Equation 10 can be solved directly for the piezometric heads ϕ at iteration *n* using the aquifer saturated thickness *h* computed from the previous iteration *n-1*. The aquifer saturated thickness is then updated with the current computed value and the piezometric heads recomputed. Approximately 5 iterations are required for convergence.

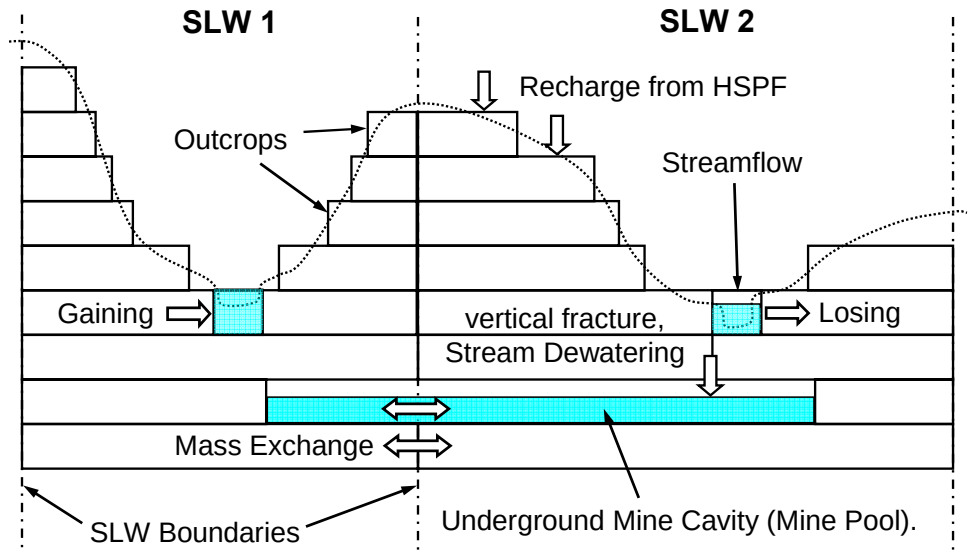

Figure 8. Hydrogeology features within a layered model structure.

RGRM Multilayer Model Structure

As illustrated in Figure 8, a multiple layer model is required to represent the subsurface structure typical of sedimentary basins. In order to include such features as perched water tables, stream and aquifer dewatering due to fractures, and the accumulation of mine pools, RGRM must have some ability to account for a vertical component of groundwater flow and its storage in layered geologic strata. To initiate progress in this direction, a multiple subsurface layer capability was added to RGRM, as shown in Figure 9. Since RGRM is intended to be computationally more efficient than MODFLOW, maintaining a 2-dimensional mathematical model structure is important. The model structure shown in Figure 9 allows vertical flow between a near surface layer and multiple subsurface layers. Specifically, a vertical leakage v_i^* [m/day] is simulated between a near surface layer and the subsurface layers through a thin confining layer located at the elevation z_i^* of the SLW stream segment outlet, as shown in Figure 10. This confining layer has a specified resistance c_i^* to vertical flow, permitting the simulation of a near surface perched water table with piezometric level ϕ_i^*, that outflows with discharge Q_i^* (Equation 3) to the local SLW stream segment. The effective volume of geologic material in the

near surface layer is approximated as a specified fraction σ_i of the computed total drainable volume of material V_i^* between elevation z_i^* and the surface.

As shown in Figure 11, a layered model structure can approximate layers of consolidated sediments typical of coal fields throughout the country. Dip in strata can be approximated by introducing elevation changes between adjacent SLWs. Layers can also change thickness and hydraulic characteristics at the SLW boundaries to approximate the in-situ variability of the actual geologic strata.

Equation 1 can be modified for application to the layered structure shown in Figure 11 by writing separate continuity equations for the near surface and subsurface layers that are solved jointly at each time step (Equations 11 and 12). The vertical leakage v_i^* provides flow connectivity between the two equations. As shown in Figure 10, the vertical leakage can be downward (drainage from the near surface layer) or upward (surcharging the near surface layer), depending on the relative elevations of the piezometric levels ϕ_i^* and ϕ_i.

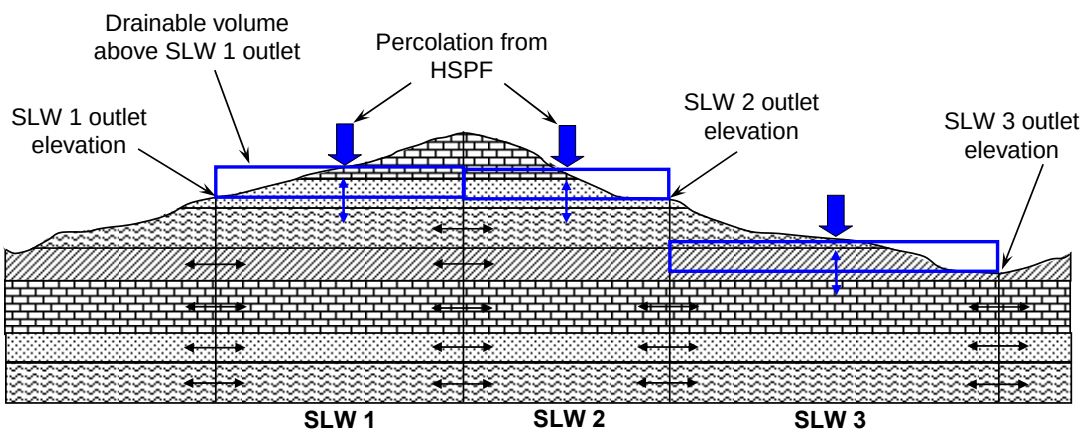

Figure 9. Layered subsurface structure within adjacent SLWs.

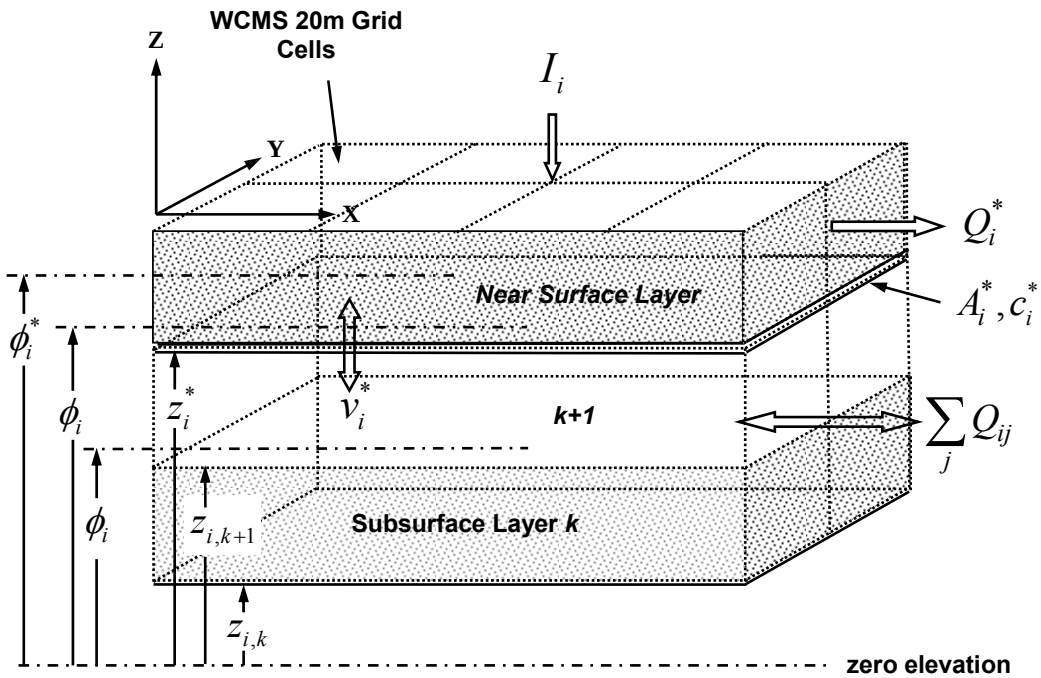

Figure 10. SLW subsurface and near surface layer structure, piezometric levels, flow balance.

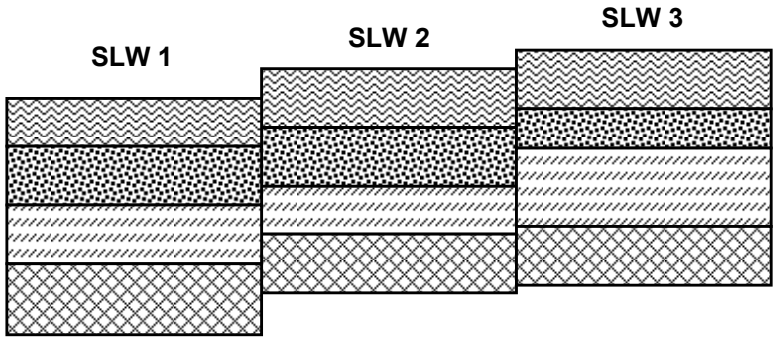

Figure 11. Representation of dip, layer thickness and heterogeneity in SLW strata.

Near Surface Layer Continuity Equation:

$$\left(I_i - v_i^*\right) A_i^* - Q_i^* = A_i^* \eta_i^* \frac{dh_i^*}{dt}$$

where:

$I_i =$ recharge rate in SLW i $\left[{}^{m}\!/_{d} \right]$

$v_i^* =$ leakage between near surface and subsurface $\left[{}^{m}\!/_{d} \right]$

$A_i^* =$ SLW i planform area $\left[m^2 \right]$

$Q_i^* =$ outflow to SLW i stream segment (see Eq. 3) $\left[{}^{m^3}\!/_{d} \right]$

$\eta_i^* =$ drainable porosity in SLW i near surface layer

$h_i^* =$ near surface layer saturated thickness in SLW i $\left[m \right]$

$t =$ time $\left[day \right]$

Note: the leakage term is conditional:

$$v_i^* = \frac{\phi_i^* - z_i^*}{c_i^*} \quad \text{if} \quad \left\{ \phi_i \le z_i^* \right\}$$

or

$$v_i^* = \frac{\phi_i^* - \phi_i}{c_i^*} \quad \text{if} \quad \left\{ \phi_i > z_i^* \right\}$$

where:

$\phi_i^* =$ piezometric level, near surface layer $\left[m \right]$

subject to: $\{ z_i^* < \phi_i^* \le \max\{\phi_i^*\} \}$

$\phi_i =$ piezometric level, subsurface layers $\left[m \right]$

$c_i^* = \dfrac{b_i^*}{K_i^*} =$ resistance of the confining layer $\left[day \right]$

$b_i^* =$ confining layer thickness $\left[m \right]$

$K_i^* =$ vertical hydraulic conductivity of confining layer $\left[{}^{m}\!/_{day} \right]$

$\max\{\phi_i^*\} = \sigma_i B_i^*$

$B_i^* = {}^{V_i^*}\!/_{A_i^*} =$ thickness of near surface layer $\left[m \right]$ (11)

$\sigma_i =$ fraction of near surface layer thickness available for storage

$V_i^* =$ drainable volume of geologic material in near surface layer $\left[m^3 \right]$

Subsurface Layers Continuity Equation:

$$\sum_j Q_{ij} + v_i^* A_i^* = A_i^* \eta_{ik} \frac{dh_i}{dt}$$

where:

$Q_{ij} =$ inflow to node i from adjacent node j (see Eq. 2) $\left[m^3 / d \right]$

$v_i^* =$ leakage between near surface and subsurface (see Eq. 13) $\left[m / d \right]$ (12)

$A_i^* =$ SLW i planform area $\left[m^2 \right]$

$\eta_{ik} =$ drainable porosity in SLW i within subsurface layer k

$h_i =$ aquifer saturated thickness in SLW i $\left[m \right]$

$t =$ time $\left[d \right]$

Horizontal hydraulic conductivities are permitted to vary from layer to layer within a particular SLW, in addition to variability between adjacent SLWs, as shown in Figures 12 and 13. No vertical hydraulic conductivities are defined within the model layers, with the exception of the confining layer separating the near surface layer from the remaining subsurface layers (K_i^* in Equation 11). The effective hydraulic conductivity K_{ij} along link *ij* between SLWs is defined as an appropriately weighted function of the two adjacent SLW hydraulic conductivities K_i and K_j as shown in Equation 13.

Unlike the 1-dimensional steady and unsteady flow formulations above, the 2-dimensional model formulation references piezometric and layer elevation levels to an arbitrary datum such as standard sea level (Figures 12 and 13). Subsurface layer thicknesses are computed from the layer bottom elevations.

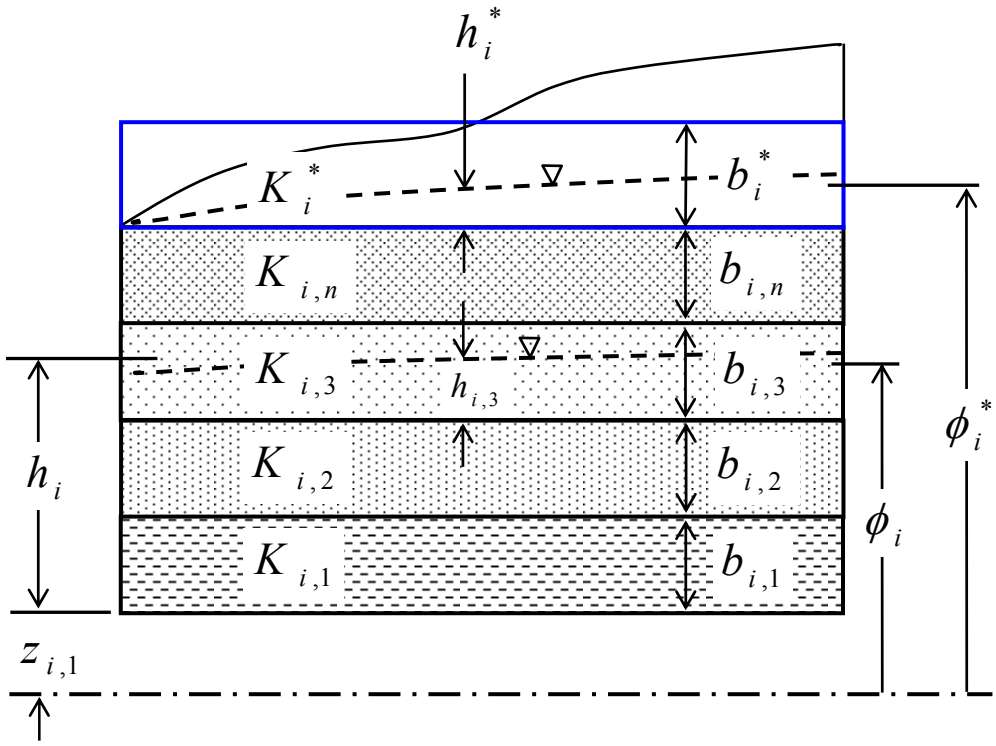

Figure 12. SLW layer properties, saturated thickness measures, and piezometric levels.

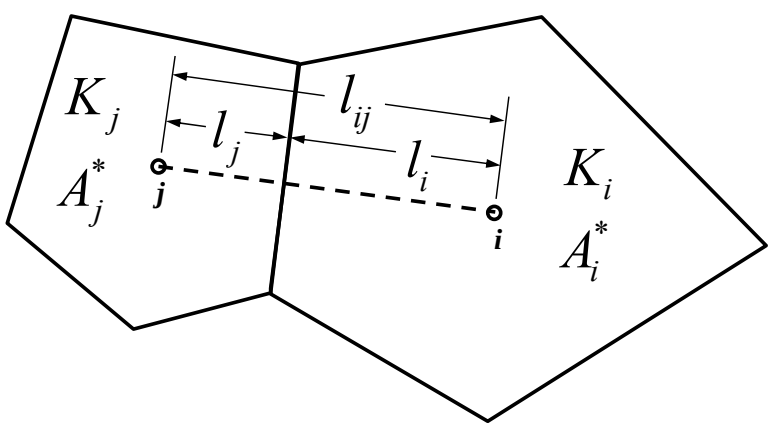

Figure 13. Computational variables in adjacent SLWs used to compute K_{ij}.

Effective Hydraulic Conductivity:

$$K_{ij} = \frac{l_{ij}}{\left[\frac{l_i}{K_i} + \frac{l_j}{K_j}\right]}$$

where:

$$l_i = \frac{l_{ij}}{\left[\sqrt{\frac{A_j^*}{A_i^*}} + 1\right]}$$

$$l_j = \frac{l_{ij}}{\left[\sqrt{\frac{A_i^*}{A_j^*}} + 1\right]}$$

$$K_i = \frac{1}{h_i}\left[\sum_{k=1}^{n-1}\left(K_{ik}b_{ik}\right) + K_{in}h_{in}\right] \qquad (13)$$

$$K_j = \frac{1}{h_j}\left[\sum_{k=1}^{m-1}\left(K_{jk}b_{jk}\right) + K_{jm}h_{jm}\right]$$

Data Analysis

Steady State Verification – Flow between Two Reservoirs

Equation 10 was implemented in MATLAB code (MATLAB, 2005) for the case of steady unconfined flow between two reservoirs. Since a square grid of node points define Voronoi polygons that are squares, this configuration (see Figure 14) was selected as best suited for this one-dimensional flow problem. The analytical solution for the saturated flow thickness *h* is Equation 14 (Bear, equation 8.1.11, page 366) which uses the Dupuit approximation (horizontal flow only).

$$h_x = \sqrt{h_{x=0}^2 - 2Qx/K}$$

where

$h_x =$ saturated flow thickness at distance $0 \le x \le L$ $\left[m\right]$

$Q =$ total discharge per unit width $\left[m^2/d\right]$ (14)

$$= \frac{K\left(h_{x=0}^2 - h_{x=L}^2\right)}{2L}$$

$K =$ hydraulic conductivity $\left[m/d\right]$

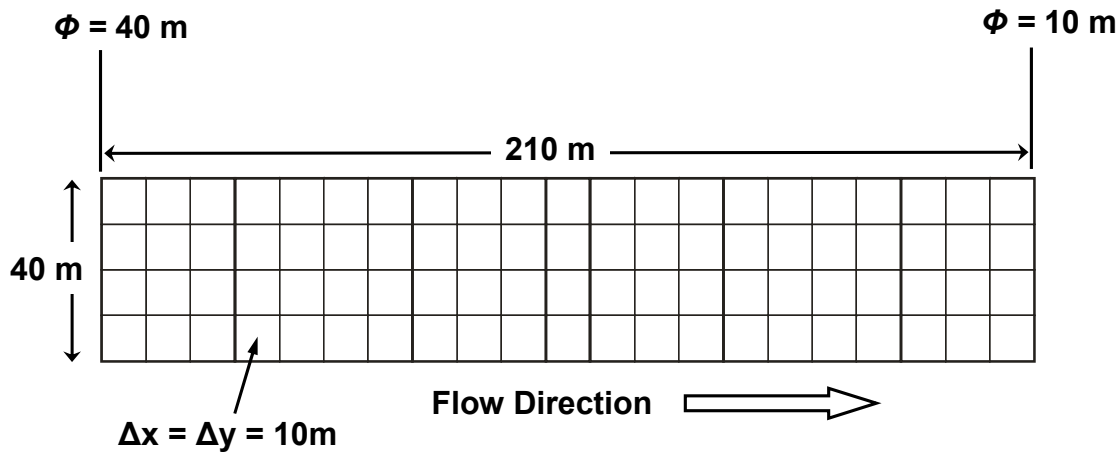

Figure 14. Square computational grid used for steady-state solution verification.

In this example the left reservoir ($x = 0$) has a depth of 40 m and the right reservoir ($x = L$) has a depth of 10 m, where $L = 210$ m (Figure 14). A square grid of 22 nodes was spaced at $\Delta x = 10$ m over the 210 m length. The width of the grid was limited to 4 nodes since the flow is entirely one-dimensional in the x-direction. The hydraulic conductivity was set constant at 1 m/day. The computed solution for the 20 interior nodes (inside the left and right boundary conditions) after 5 iterations was essentially identical to that predicted by Equation 14. The RMS error of the computed saturated flow thickness (head) was $1.3796e^{-6}$ m.

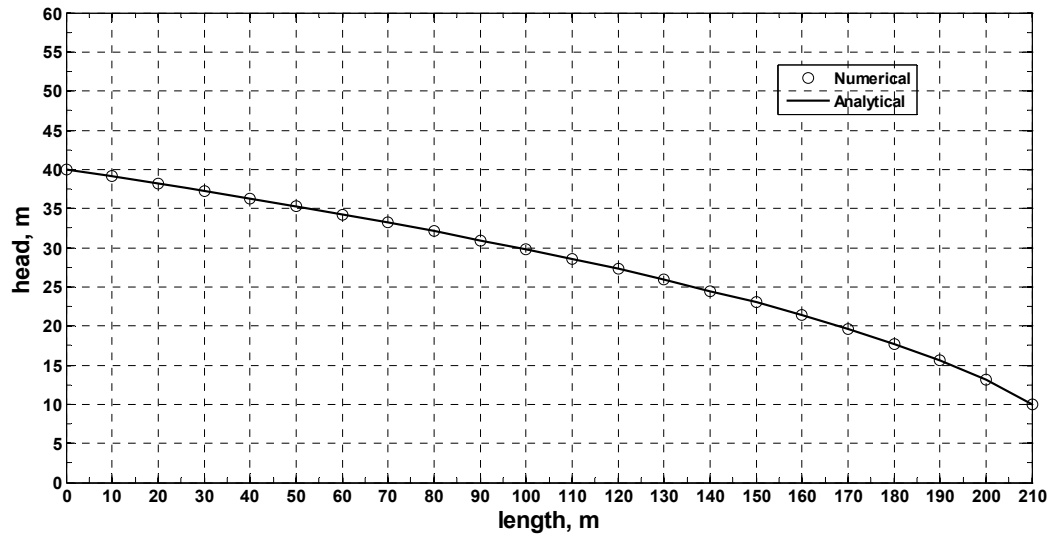

Figure 15. Comparison of steady state numerical solution to analytical solution for unconfined flow between two reservoirs.

Steady State Verification – Flow between Two Reservoirs with Recharge

The MATLAB program used for the unconfined flow between two reservoirs above was already configured with the capability to add a nonzero uniformly distributed recharge. A recharge of rate $I = 0.1\ [m/d]$ was added. The analytical solution for the steady state flow between two reservoirs (with recharge added) is given by Equation 15 (Bear, 1972, equation 8.2.18, pages 379-380). The numerical result is compared to the analytical result as shown in Figure 16. The computed solution for the 20 interior nodes (inside the left and right boundary conditions) after 8 iterations was essentially identical to that given by Equation 15. The RMS error of the computed saturated flow thickness (head) was 1.18e^{-4} m.

$$h_x = \left[h_{x=0}^2 - \frac{h_{x=0}^2 - h_{x=L}^2}{L} x + \frac{I}{K}(L - x)x \right]^{1/2}$$

where

h_x = saturated flow thickness at distance $0 \le x \le L\ [m]$ (15)

I = recharge rate $[m/d]$

K = hydraulic conductivity $[m/d]$

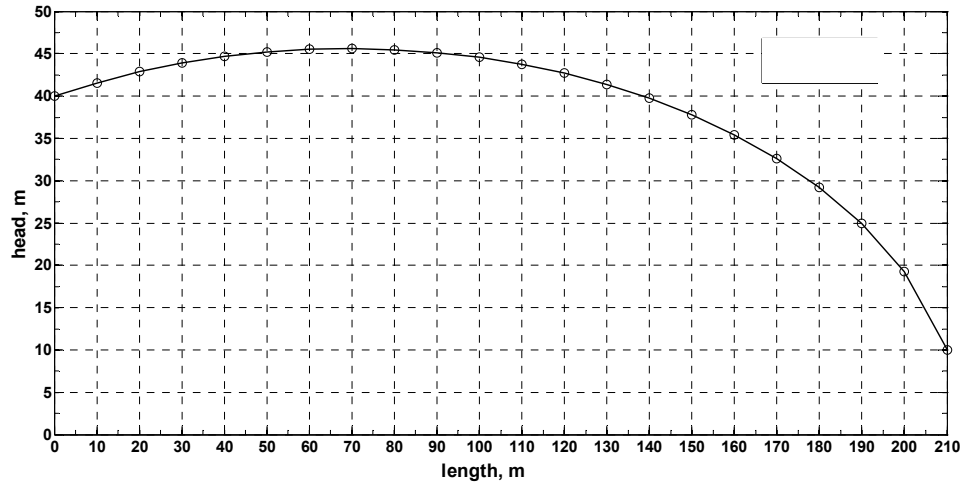

Figure 16. Comparison of steady state numerical solution to analytical solution for unconfined flow between two reservoirs, with recharge.

Unsteady Flow Solution Verification

Following verification of the steady state solution, Equation 6 (the unsteady finite difference equation) was coded in MATLAB for testing against the same two reservoir case above using the same grid dimensions (Figure 14). But unlike the steady state solution, cyclic boundary conditions were imposed in the grid direction normal to the direction of flow. Since the grid has four columns (nodes) in the normal direction, the first column of nodes and the fourth column of nodes must be connected with a flow link normal to the flow direction (along the grid rows). In terms of grid geometry, this is analogous to rolling the grid into a cylinder so that the first and fourth columns of the grid can be connected together. Cyclic conditions are required to properly simulate a one dimensional flow in the vertical plane since, mathematically, the flow is assumed to extend infinitely into and out of the plane of the paper.

The verification test consisted of starting the simulation with initial conditions shown in Figure 17 at t = 0. All interior grid nodes were initialized to a head of 40 m (same as the fixed reservoir head on the left) except for the last grid row on the right which corresponded to the fixed 10 m reservoir head. The hydraulic conductivity remained the same (1 m/day) and the drainable porosity η (equal to the specific yield S) was set equal to 0.2. The solution was computed for variable times and time increments to explore the solution characteristics. A time increment of 1 day was found to produce divergent errors (instability). A time increment of 0.1

day was found to give good results (it is noted that a later computer code correction eliminated the instability problem when using daily time increments). A total simulation time of about 2000 days (20,000 time steps) was required for the numerical solution to approach the steady state analytical solution. As shown in Figure 17 the numerical solution at this point in time was indistinguishable from the analytical solution. When Equation 6 is solved for the collapse of the piezometric surface to a steady state, as shown in Figure 17, the saturated thickness between nodes will approach the correct value as the transient solution converges to the steady state solution.

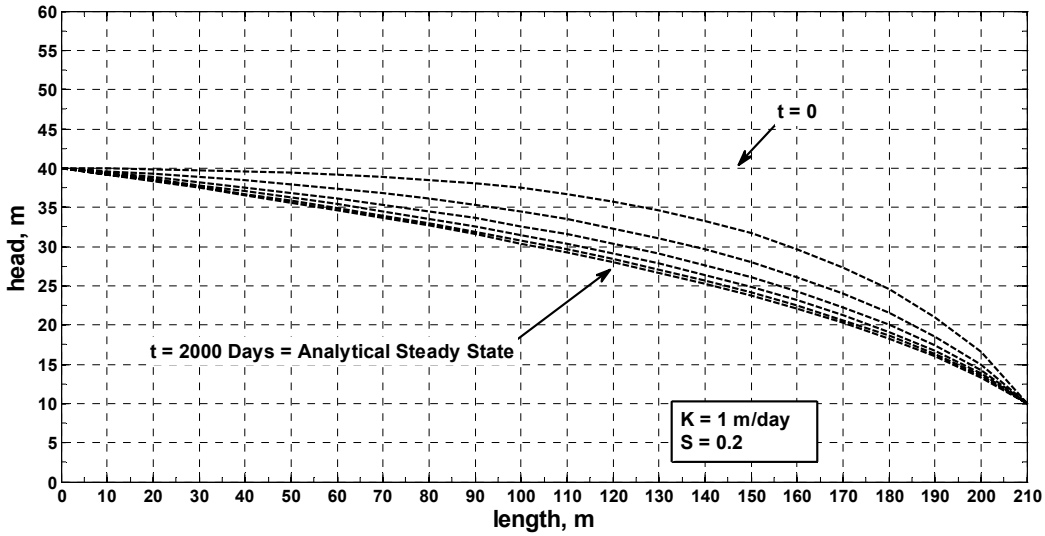

Figure 17. Unsteady flow numerical solution: from horizontal water table to the steady state analytical solution shown in Figure 15 (plotted at Δt = 200 days).

The next unsteady flow verification test used a time-dependent analytical solution consisting of a declining piezometric surface between to parallel drains (Bear, 1972, equation 8.2.43, pages 381-383). Equation 16 is the analytical solution which uses the Dupuit approximation.

$$h(x,t) = \frac{h_0(x)}{\left[1 + \left(\beta K\, h_0(L)\, t\right) / \left(\eta L^2\right)\right]}$$

where

$$h_0(x) = h_0(L) F(x/L)$$

$$F(x/L) = \left(1.321 - 0.142\left(x/L\right) - 0.179\left(x/L\right)^2\right)\sqrt{\left(x/L\right)} \tag{16}$$

$$\beta = 1.12$$

$K =$ hydraulic conductivity

$\eta =$ drainable porosity

$t =$ time

As shown in Figure 18, the x axis origin is at the left drain location and extends to the axis of symmetry where $x = L$. The opposite side (extending on to the right drain) is a mirror image of the left side of the solution domain. The solution at $t = 0$ is solved first by selecting a value of $h_0(L)$ and solving for the corresponding head values $h_0(x)$ using lower portion of Equation 16. The solution for heads $h(x,t)$ can then be computed using the top relationship in Equation 16 at any desired time t. The analytical solution and numerical model are set up for $L = 210$ m and $h_0(L) = 40$ m, therefore there are 43 grid rows (nodes) spaced at 10 m in the numerical model. As before, there are four columns (four nodes in width) in the numerical grid. Again, cyclic boundary conditions are used, linking column one to column four. The simulation was run for a total of 500 days using daily time increments. As shown in Figure 19, the numerical solution (points) show excellent agreement with the analytical solution (lines) given by Equation 16. The rms errors are listed in Table 1.

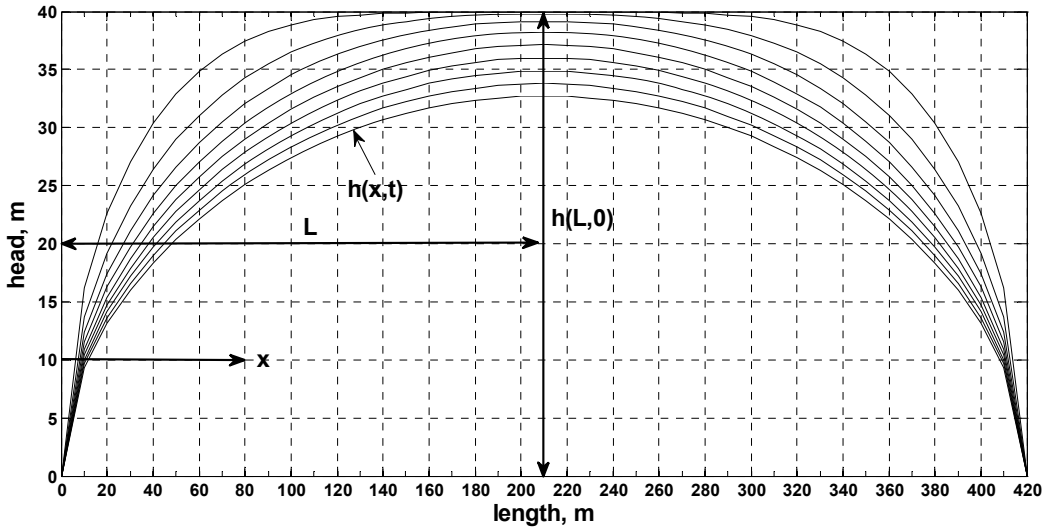

Figure 18. Declining piezometric head between parallel drains: analytical solution domain variables.

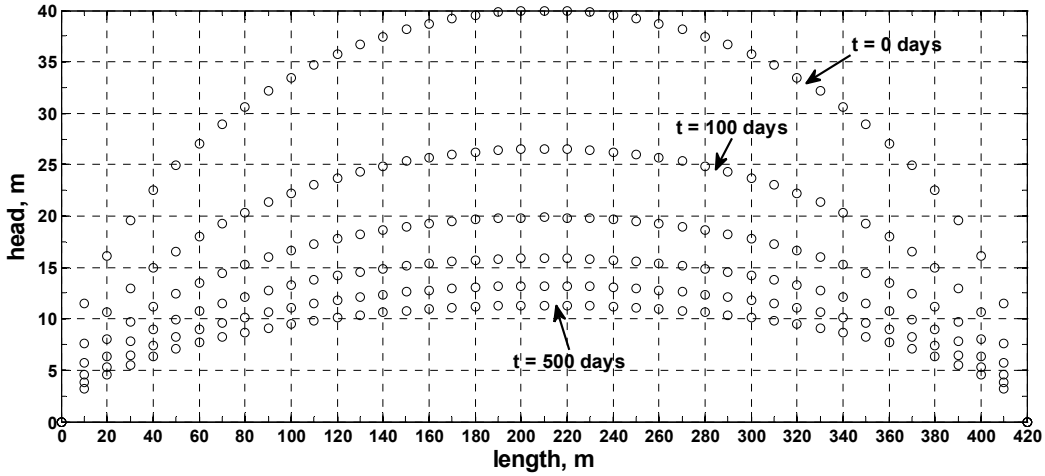

Figure 19. Declining piezometric head between parallel drains: numerical solution (points) versus analytical solution (lines).

Table 1. RMS error results for the numerical solution shown in Figure 19.

Time, Days	rms error, m
100	0.024892
200	0.027767
300	0.027570
400	0.026344
500	0.024836

Steady State - Multiple Layer Verification

The steady state model grid shown in Figure 14 above was modified so that three geologic layers could be simulated, each with individual values of hydraulic conductivity. An analytical solution for two layers was available for use in verification, but not for three. To match the three layer numerical model to the available analytical model, the first two layers were assigned the same hydraulic conductivity value so that it was functionally a single layer. The bottom layer was 20 m thick (K=0.5 m/d) and the top layer 25 m thick (K=1.0 m/d). The horizontal equivalent hydraulic conductivity was calculated using Equation 13. The left boundary condition was a fixed head of 40 m and the right boundary at 30 m. The analytical solution is given by Equation 17 (Eq. 8.1.31, pg 370, Bear, 1972).

$$Q = \frac{K''}{2L}\left(h_0 - h_L\right)\left[h_0 + h_L - 2a + 2\frac{K'}{K''}a\right] \tag{17}$$

where

K' = hydraulic conductivity of layer 1 (bottom) [m/d]

K'' = hydraulic conductivity of layer 2 (top) [m/d]

h_0 = left boundary condition fixed head [m]

h_L = right boundary condition fixed head [m]

L = horizontal length between left and right fixed heads [m]

a = thickness of layer 1 [m]

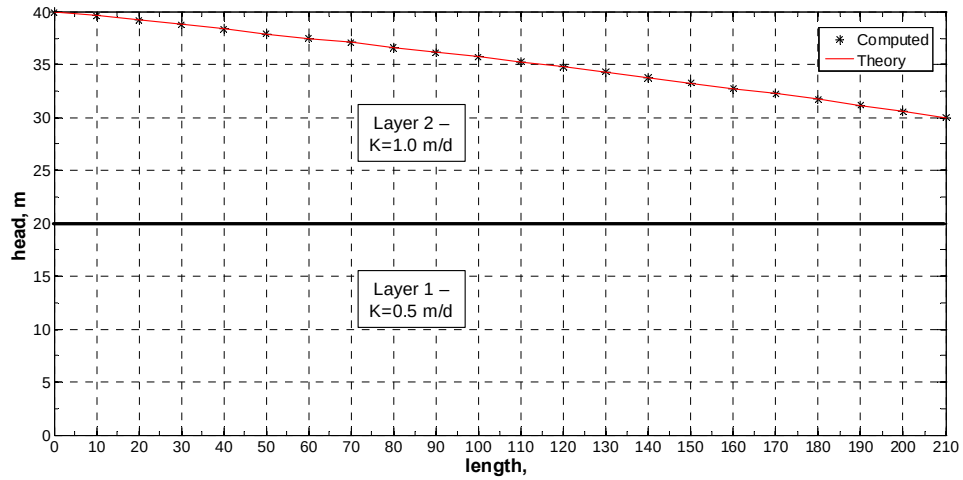

Figure 20. Comparison of steady state numerical solution to analytical solution for unconfined flow between two reservoirs, with two geologic layers.

The rms error of the computed compared to theory in Figure 20 is $4.7459e^{-5}$ m after 5 iterations, which indicates a near exact agreement with theory.

Results

Following verification of the RGRM model as outlined in the previous section, a performance comparison with GMS-MODFLOW was conducted. A three layer model was constructed in GMS as shown in Figure 21. The grid size is 20 x 20 grid cells, covering a 10,000 m square flow domain. Each grid cell is 500 m square. The three layers begin at elevation zero and each is 100 m thick for a total depth of 300 m. The horizontal hydraulic conductivities were 1, 3, and 5 m/d from the bottom to the top layer. Vertical anisotropy was set to 1.0 for all layers. As shown in Figure 21, the Left column is a fixed head of 250 m. The left hand boundary column in Figure 21 is at a fixed head of 250 m. The top, bottom, and right side boundaries of the grid are groundwater barriers with no inflow-outflow. A series of drains extends along row 9 from the left fixed head boundary for 12 cells distance. The drain elevations range from 250 m to 275 m from left to right. The recharge rate is 0.001 m/day uniformly over the total grid area. The RGRM model duplicated all aspects of this grid. Figure 22 shows the corresponding heads generated in the RGRM model. It should be noted that Figure 22 is mirror image of Figure21 about the row direction (rows are plotted in reverse order due to plotting software limitations).

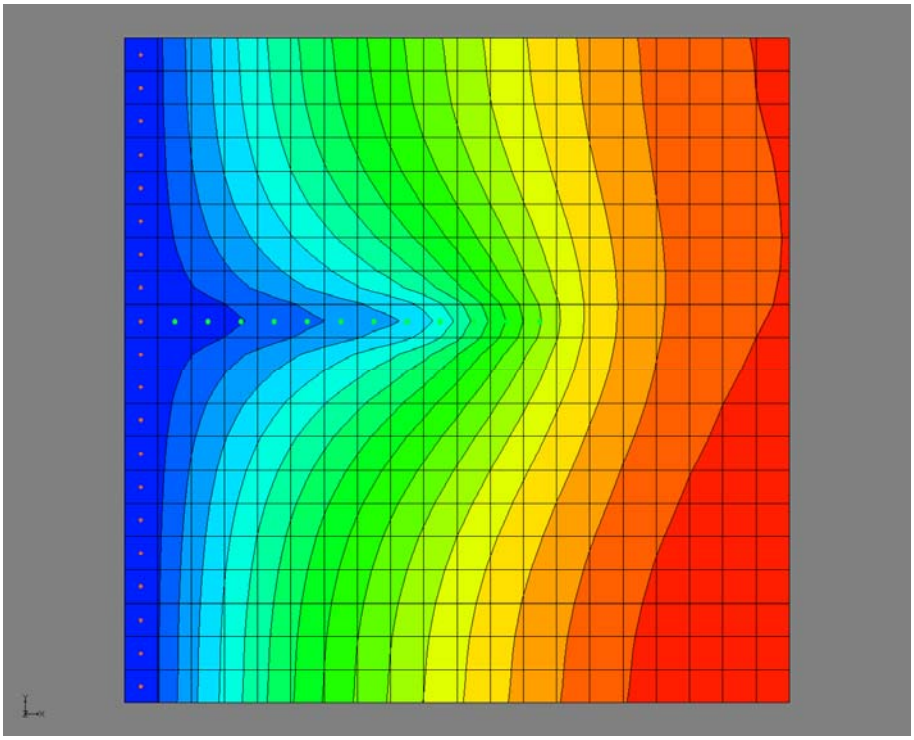

Figure 21. GMS-MODFLOW three layer 20 x 20 cell grid with head contours.

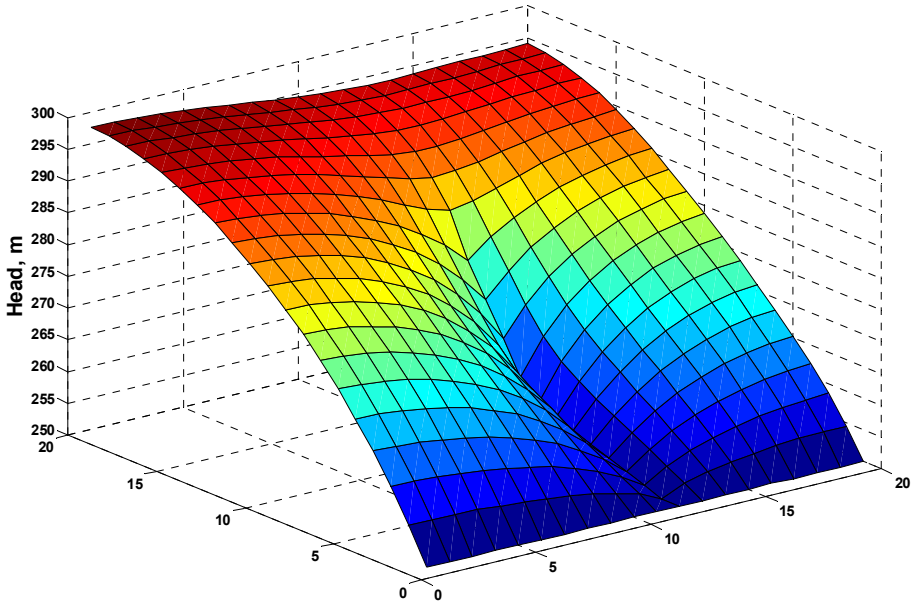

Figure 22. Computed heads in the RGRM three layer 20 x 20 grid cell model.

The major difference between the two simulations shown in Figures 21 and 22 is that MODFLOW simulates vertical groundwater flow in addition to horizontal flow (full 3-D simulation) while RGRM can only simulate the horizontal component. This disparity produces the largest potential errors in the presence of groundwater barriers, of which there are three on each of three sides of the flow domain. Groundwater barriers do not allow horizontal flow, therefore flow can only be vertical against the barrier (as a result of surface recharge). Since RGRM cannot simulate vertical flow, this example serves as the most severe test of error potential in the model. A comparison of heads in the uppermost layer reveals significant errors. The corner grid cell where the barriers meet at right angles (upper right corner in Figure 21) demonstrates the largest error. The MODFLOW head in this corner cell is 280 m, while the corresponding head in RGRM is 298 m, an error of 18 m. In the other corner (bottom right in Figure 21) the error is 14 m. The remaining errors in the grid range proportionally downward toward the fixed heads and drains. The approximate rms error for the entire grid is 7 m.

Conclusions

The RGRM modeling concept was based on the desire to couple the HSPF surface water modeling system with a groundwater modeling component that would be useful in analyzing the impacts of underground mining on groundwater systems. It was hypothesized that a simplified 2-D model would be adequate for most of the areas simulated as opposed to a full 3-D model like MODFLOW. The RGRM model was proven to perform perfectly in comparisons with 2-D analytical solutions from the literature. However, when subjected to a typical 3-D problem, large errors were experienced in the RGRM model when compared to MODFLOW. It is concluded that the 2-D RGRM model is inadequate to simulate the complex flows with vertical components that would be experienced near underground mining operations. Therefore, it remains for future work to add a suitable vertical flow component to the current RGRM 2-D model to give it at least a partial 3-D capability. Since future funding has been denied, it is doubtful that RGRM will be developed to a point where it can demonstrate its value as a usable groundwater modeling component of the WCMS-HSPF hydrologic modeling system.

Acknowledgements

The authors express their appreciation for the support of the West Virginia Department of Environmental Protection and the U.S. Dept. of Interior Office of Surface Mining, Reclamation

and Enforcement, under the Applied Science Cooperative Agreement Program, Cooperative Agreement Number S07AZ12498.

Literature Cited

Bicknell, B.R. et al. 2001. Hydrological Simulation Program - Fortran, HSPF Version 12 User's Manual. U.S. EPA. Athens, Georgia.

Bear, Jacob 1972. Dynamics of Fluids in Porous Media. Environmental Science Series. American Elsevier Publishing Co., Inc. New York.

Bear, Jacob, and Verruijt, Arnold; 1987. Modeling Groundwater Flow and Pollution. D. Reidel Publishing Company. Boston, Mass.

Capo, Rosemary C., 2004. Evolution of Historically Acidic Mine Drainage (AMD) to Alkaline Discharges: Irwin Coal Basin, Pennsylvania. 2004 Denver Annual Meeting. Geological Society of America. Paper No. 99-5. Denver, CO. November 7-10.

Eli, Robert N.; Fletcher, Jerald J.; Galya, Thomas A.; Strager, Michael P.; Lamont, Samuel J.; Sun, Quingyun; Churchill, John B.; 2004. Hydrologic Modeling Tools for Cumulative Hydrologic Impact Assessment of West Virginia Coal Mine Permits. Advanced Integration of Geospatial Technologies in Mining and Reclamation. US Dept. of Interior Office of Surface Mining. Atlanta, Georgia. December 7-9.

Eli, Robert N.; Fletcher, Jerald J.; 2005. Cumulative Hydrologic Impact Assessment of West Virginia Coal Mine Permits Using HSPF and WCMS. Watershed Management Conference 2005: Managing Watersheds for Human and Natural Impacts, Engineering, Ecological, and Economic Challenges. American Society of Civil Engineers. Williamsburg, Virginia. July 19-22.

Fletcher, Jerald J.; Eli, Robert N.; Galya, Thomas A.; Strager, Michael P.; Lamont, Samuel J.; Sun, Quingyun; Churchill, John B.; Schaer, Andrew N.; 2004. The Watershed Characterization and Modeling System (WCMS): Support Tools for Large Watershed CHIA and NPDES Analyses. Advanced Integration of Geospatial Technologies in Mining and Reclamation. US Dept. of Interior Office of Surface Mining. Atlanta, Georgia, December 7-9.

Harbaugh, A.W., 2005, MODFLOW-2005, The U.S. Geological Survey Modular Ground-Water Model—The Groundwater Flow Process. U.S. Geological Survey Techniques and Methods 6-A16.

Lamont, Samuel; Eli, Robert; Fletcher, Jerald J.; 2005. The Calibration of a Complex Watershed Model in Sparse Data Environments – Use of Supplemental Indices. Watershed Management Conference 2005: Managing Watersheds for Human and Natural Impacts. Engineering, Ecological, and Economic Challenges. American Society of Civil Engineers. Williamsburg, Virginia. July 19-22.

MATLAB, Version 7, 2005. The Mathworks, Inc. www.mathworks.com.

Narasimhan, T.N. and Witherspoon, P.A. 1976. An Integrated Finite Difference Method for Analyzing Fluid Flow in a Porous Media. Water Resources Research. 12, pgs. 57-64.

Pozrikidis, C. 1998. Numerical Computation in Science and Engineering. Oxford University Press, New York, N.Y.

Ross, Mark; Geurink, Jeffrey; Aly, Alaa; Tara, Patrick; Trout, Ken; and Jobes, Tom; 2004. Integrated Hydrologic Model (IHM), Volume I: Theory Manual. Intera Inc., University of South Florida. Aqua Terra Consultants.

Sahu, Parameswar, 2003. Modeling Groundwater Flow in Abandoned Underground Coal Mines of the Corning Mine Complex, Perry County, Ohio. 2003 Seattle Annual Meeting. Geological Society of America. Paper No. 252-4. Seattle, WA. Nov. 2-5.

Strack, Otto D. L., 1988. Groundwater Mechanics. Prentice-Hall, Inc. Englewood Cliffs, New Jersey.

USEPA, 2001. User's Manual: Better Assessment Science Integrating Point and Nonpoint Sources: BASINS Version 3.0, EPA-823-B-01-001, U.S. Environmental Protection Agency, Washington, D.C.